The new ternary silicide Gd5CoSi2: Structural, magnetic and magnetocaloric properties

Charlotte Mayer, Etienne Gaudin, Stéphane Gorsse, Bernard Chevalier

The new ternary silicide Gd_5CoSi_2 : structural, magnetic and magnetocaloric properties

Mayer C., Gaudin E., Gorsse S., Chevalier B.

Abtract : Gd_5CoSi_2 was prepared by annealing at 1003 K. Its investigation by the X-ray powder diffraction shows that the ternary silicide crystallizes in a tetragonal structure deriving from the Cr_5B_3-type (*I*4/*mcm* space group; *a*=7.5799(4) and *c*=13.5091(12) Å as unit cell parameters). The Rietveld refinement shows a mixed occupancy on the (8*h*) site between Si and Co atoms. Magnetization and specific heat measurements performed on Gd_5CoSi_2 reveal a ferromagnetic behaviour below T_C=168 K. This magnetic ordering is associated to an interesting magnetocaloric effect; the adiabatic temperature change ΔT_{ad} is about 3.1 and 5.9 K, respectively, for a magnetic field change of 2 and 4.6 T.

1. Introduction :

Since the discovery of interesting magnetocaloric effect (MCE) around the room temperature, for the gadolinium [1] and giant MCE in the pseudo-binary compound $Gd_5Si_2Ge_2$ [2], research of new ferromagnetic compounds exhibiting such huge effect has exploded. Indeed, an MCE can be used in the magnetic refrigeration as a potential alternative for conventional gas-compression/expansions refrigeration technology. It was shown that when the ferromagnetic ordering is coupled to a first-order structural transition as for $Gd_5Si_2Ge_2$, the large MCE is usually accompanied with important magnetic and thermal hysteresis, which induces a low working efficiency for applications in magnetic refrigeration [2], [3] and [4]. In this view, as it is rather difficult to introduce and control structural transformations in materials, it is of great interest to optimize an MCE due to the magnetic transition only. In general, large MCE is associated with the use of elements that have a high magnetic moment per atom like rare earths (*RE*) and some 3*d* transition metals (Fe, Co).
Considering these arguments, we have recently started the investigation of the *RE*–Co–Si ternary systems and discovered the intermetallics $RE_6Co_{1.67}Si_3$ with *RE*=La, Ce, Nd, Gd, Tb and Dy [5], [6], [7], [8] and [9]. These ternary silicides crystallize in an hexagonal structure [7] deriving from that of the binary compound $Gd_6Co_{4.85}$ [10] and no solid solution between these two last intermetallics was evidenced. The $RE_6Co_{1.67}Si_3$ compounds exhibit interesting magnetic properties: (i) $Gd_6Co_{1.67}Si_3$ orders ferromagnetically at 294 K, a Curie temperature comparable to that observed for pure gadolinium and exhibits a reversible second-order magnetic transition inducing a remarkable MCE [6], [11], [12] and [13] and (ii) two successive ferro(ferri)magnetic transitions appear below T_C=84 and 186 K for $Nd_6Co_{1.67}Si_3$ and $Tb_6Co_{1.67}Si_3$, respectively [8], [9], [11], [14], [15], [16] and [17]. Moreover during the determination of the magnetic structures of these last ternary silicides using neutron powder diffraction [8], we have reported for the first time on the existence of the RE_5CoSi_2 (*RE*=Nd and Tb) compounds, revealed as impurities by this study. Following this work, we carried on the investigation in the Gd–Co–Si system and synthesized the new ternary silicide Gd_5CoSi_2. Its existence was not evidenced in the most recent paper devoted to the equilibrium phase diagram at 773 K in the Gd–Co–Si system [18].
In this paper, we present and discuss the crystallographic, magnetic, thermal and magnetocaloric properties of Gd_5CoSi_2. They are compared to that of other ternary and binary compounds existing in the ternary Gd–Co–Si system.

2. Experimental

Polycrystalline Gd_5CoSi_2 ingots were prepared by arc-melting precisely weighted stoichiometric mixture of high purity elements Gd, Co (99.9%) and Si (99.9999%) in a purified argon atmosphere. Melting was performed several times to ensure a good homogeneity. The weight loss during this process was less than 0.2 wt%. Annealing was finally performed at 1003 K for 1 month on the sample enclosed in evacuated quartz tubes. No reaction between the sample and the quartz tube was observed.
Both the composition and homogeneity of the annealed sample were checked by microprobe analysis using Cameca SX-100 instrument. The analysis was performed on the basis of intensity measurements of Gd-Lα_1, Co-Kα_1 and Si-Kα_1 X-rays emission lines, which were compared with those obtained for high purity elements Gd, Co and Si used as reference compounds.

X-ray powder diffraction was performed with the use of a Philips 1050-diffractometer (Cu-Kα radiation) for the phase identification of the as-cast and annealed samples. X-ray powder diffraction data for the characterization of the structural properties of the Gd_5CoSi_2 annealed sample were collected with a Philips X-Pert diffractometer operating at room temperature and using Cu-Kα_1 radiation (λ=1.54051 Å). The powder diffraction pattern was scanned over the angular range 7.512–119.992° with a step size of $\Delta(2\theta)$=0.008°. Rietveld refinement was performed using the Jana2006 program package [19]. The background was estimated by a Legendre function with 12 parameters, and the peak shapes were described by a Lorentzian function for Gd_5CoSi_2. A correction for roughness (Bragg-Brentano geometry) and absorption correction were introduced to avoid negative value of the atomic displacement parameters (ADPs) induced by the high absorption coefficient of the sample.

Magnetization measurements were performed using a superconducting quantum interference device (SQUID) magnetometer (Quantum Design MPMS-XL) in the temperature range 5–320 K and applied fields up to 4.6 T. Heat capacity was determined with a standard relaxation method with a QD PPMS device. Samples of approximately 40 mg were glued to the sample holder using Apiezon N-grease. The heat capacity of the sample holder and grease was measured just before the sample was studied.

3. Results and discussion

3.1. Synthesis and structural properties

The analysis of the as-cast sample by X-ray powder diffraction is presented in Fig. 1 and reveals the presence of three phases: the binaries Gd_5Si_3 [20] and Gd_3Co [21] compounds and the $Gd_6Co_{1.67}Si_3$ ternary silicide [5]. On the contrary, after annealing at 1003 K (temperature determined after several experiments in accordance with melting temperatures of the phases existing in an as-cast sample) for one month, the Gd_3Co phase has totally disappeared and the new ternary Gd_5CoSi_2 silicide has formed. Some amounts of Gd_5Si_3 and $Gd_6Co_{1.67}Si_3$ also remain as impurities (Fig. 1).

The back-scattered electrons image (microprobe analysis) presented in Fig. 2 confirms the presence of a main phase with 63.8(7)% of Gd, 11.5(2)% of Co and 24.7(4)% of Si as experimental atomic percentages, close to those expected for the exact Gd_5CoSi_2 stoichiometry (62.5% of Gd, 12.5% of Co and 25% of Si) and some traces of $Gd_6Co_{1.67}Si_3$ and Gd_5Si_3 impurities. Moreover the boundaries between the Gd_5Si_3 and Gd_5CoSi_2 domains visible on this image are strictly defined, thus excluding the existence of a solid solution between these two compounds. In other words, the solid solution $Gd_5(Si_{1-x}Co_x)_3$ does not exist; Gd_5Si_3 and Gd_5CoSi_2 are in equilibrium at 1003 K.

Analysis of the X-ray powder diffraction pattern (Fig. 3) of the annealed sample shows that the ternary silicide Gd_5CoSi_2 crystallizes in the tetragonal Cr_5B_3-type structure (space group *I*4/*mcm*) with the refined unit cell parameters *a*=7.5799(4) and *c*=13.5091(12) Å. The impurity phases Gd_5Si_3 [20] and $Gd_6Co_{1.67}Si_3$ [5] were taken into account with a determined amount equal to 1.2 and 2.7 wt%, respectively. A first model with only silicon atoms in the 4*a* and 8*h* sites was used and led to the Debye–Waller factors U_{iso}=0.038(14) Å^2 for the 4*a* site and 0.001(6) Å^2 for the 8*h* site. Mixing of cobalt on both sites was also tested and the sum of their occupancy factors was constrained to be in agreement with the overall composition. A decrease of the occupancy factor of cobalt down to 0 was observed for the 4*a* site concomitantly to an increase up to 50% in the 8*h* site. The filling of the 4*a* site only by cobalt atoms was also tested and the U_{iso} parameter of cobalt exceeded the value of 0.2 Å^2. All these attempts proved undoubtedly that the cobalt atoms are localized on the 8*h* site. The occupancy ratio of Co and Si on this last position was fixed to 0.5 to fulfill the composition and the ADPs of the lighter elements, Co and Si, were constrained to be equal to avoid high correlations in the refinement. The final refinement of the atomic positions with isotropic ADPs led to the profile factors R_p/R_{wp}=2.70/3.63% and the reliability factors $R_{F(obs)}/R_{B(obs)}$=5.56/10.47%. The profile refinement is displayed in Fig. 3; the atomic positions with isotropic ADPs are gathered in Table 1 and the interatomic distances in Table 2.

In the tetragonal Cr_5B_3-type structure, boron atoms are located on the two 8*h* and 4*a* *Wyck*off positions. In Gd_5CoSi_2, a statistical distribution of Co and Si1 atoms on the 8*h* *Wyck*off position is observed, the 4*a* position being only filled by Si2 atoms (Fig. 4). This structure can be described as reported previously for Nd_5Si_3 [22] by the alternate stacking of two different slabs along the *c*-axis: the first one (Gd_3CoSi) of U_3Si_2-type consists of tetragonal [$Gd2_8$] prisms filled with Gd1 atoms, and pairs of face-sharing trigonal [$Gd2_6$] prisms filled with the Co/Si1 mixture, and the second one (GdSi)

consists of tetragonal [$Gd2_8$] antiprisms filled with Si2 atoms, and pairs of edge-sharing empty [$Gd2_4$] tetrahedra. Similar structure was reported for the compounds $La_5Co_{0.3}Si_{2.7}$ and $Nd_5Co_{0.31}Si_{2.69}$ [23].

In the sequence $Gd_5Si_3 \rightarrow Gd_5CoSi_2$, we observe a change of structure from Mn_5Si_3-type (Gd_5Si_3) to Cr_5B_3-type (Gd_5CoSi_2). As in this case, a stabilization of the Cr_5B_3-type structure was observed in the past for $Gd_5Co_{1.73}Bi$ [24], Gd_5Ni_2Bi, Gd_5Pd_2Bi [25] and Gd_5Au_2Bi [26] through the substitution of Bi by a transition element in Gd_5Bi_3, which crystallize with the Mn_5Si_3-type structure [27]. In all these compounds, the smaller atoms (Co, Ni, Pd, Au) occupy preferentially the 8*h* site, whereas the bigger Bi atoms are located on the 4*a* site. Similar remark can be made for Gd_5CoSi_2 since the smaller Co atoms (the metallic radius *r* give r_{Co}=1.252 Å<r_{Si}=1.319 Å [28]) occupy partially the 8*h* site.

In Gd_5CoSi_2, the mixture Co/Si1 (8*h* site) is located in trigonal [Gd_6] prisms as observed for Si atoms in Gd_5Si_3 [20], and Si and Co2 atoms in $Gd_6Co_{1.67}Si_3$ [5]. The average Co/Si1-Gd2 distance of 2.96 Å determined here for Gd_5CoSi_2 (Table 2) is between those of Si–Gd reported for Gd_5Si_3 (3.025 Å) and $Gd_6Co_{1.67}Si_3$ (3.07 Å) and those of Co2–Gd existing in $Gd_6Co_{1.67}Si_3$ (2.932 Å). Also, it is interesting to note that the average distance Co/Si1-Gd2 (2.960 Å) is smaller than that of Si2–Gd2 (3.163 Å) in agreement with the fact that the smaller Co atoms occupy the smaller 8*h* site. The Gd–Gd distances vary from 3.362 to 3.987 Å and most of them are smaller than the sum of metallic radii (3.604 Å) (Table 2). This behaviour suggests the existence of strong Gd–Gd magnetic interactions in the ternary silicide Gd_5CoSi_2.

3.2. Physical properties

Fig. 5 shows the temperature dependence of the zero-field cooled (ZFC) and field cooling (FC) magnetization *M* of Gd_5CoSi_2 (annealed sample) measured with an applied field of 0.05 T. These curves display two rather sharp increases in *M* at the Curie temperatures T_{C1}=298 K and T_{C2}=168 K (temperatures defined as the extrema of the derivative curve *dM*/*dT* versus *T*). The first small increase at T_{C1} corresponds to the ferromagnetic ordering of the impurity phase $Gd_6Co_{1.67}Si_3$ [5]. The second increase, at T_{C2}=168 K, also indicates the occurrence of a ferromagnetic ordering that can be attributed to the new phase Gd_5CoSi_2. Above 320 K, the reciprocal magnetic susceptibility χ_m^{-1} of Gd_5CoSi_2, measured with an applied field of 3 T (inset of Fig. 5), follows Curie Weiss law. The experimental value of the effective magnetic moment μ_{eff}=7.95 μ_B/Gd is close to the calculated value for a free Gd^{3+} ion (7.94 μ_B/Gd). This suggests that Co is nonmagnetic in this ternary silicide.

These magnetization measurements indicate that the partial replacement of an Si by Co atoms in Gd_5Si_3 induces a modification of the magnetic behaviour from antiferromagnetism to ferromagnetism. Indeed, Gd_5Si_3 orders antiferromagnetically below T_N=55 K [29], whereas as determined here Gd_5CoSi_2 exhibits a ferromagnetic behaviour below 168 K. Similar remark was claimed previously during the replacement of Bi by Ni atoms in Gd_5Bi_3; strong antiferromagnetic interactions exist in Gd_5Bi_3 [30], but the compound $Gd_5Ni_{0.71}Bi_{2.29}$ presents a ferromagnetic ordering below 162 K [31]; a Curie temperature close to that observed for Gd_5CoSi_2.

The temperature dependence of the specific heat Cp of Gd5CoSi2 measured in zero magnetic field is shown in Fig. 6. The Cp versus T curve exhibits two λ-type peaks at 295 and 165 K; temperatures defined by the maximum of the peaks. These results are in an excellent agreement with the magnetization data and confirm the presence of a magnetic transition near 168 K for Gd_5CoSi_2. According to the Dulong–Petit law, only the lattice contribution to Cp(T) is effective at high temperature. The Cp limit of a compound with n atoms per unit cell must then be equal to the theoretical value of 3nR, with R=8.31 J mol^{-1} K^{-1} the gas constant. For Gd_5CoSi_2, this calculated value is equal to 199.4 J mol^{-1} K^{-1} (n=8), which is 13% less than the measured one of 229.5 J mol^{-1} K^{-1} at 312 K. The exceeding value is probably attributable to the magnetic contribution of the impurity $Gd_6Co1_{.67}Si_3$, which presents a Curie temperature around 298 K [5] and we can assume that the Gd_5CoSi_2 ternary silicide brings only its lattice contribution to Cp. As the existence of the non-magnetic isomorphous compounds La_5CoSi_2 and Y_5CoSi_2 is not reported in the literature and our attempts to synthesize them were not successful, the only way to estimate the magnetic contribution Cm is to estimate and subtract both electronic contribution Cel and lattice (phonon) contribution Clat to the measured Cp. Cel is fitted linearly at low temperatures and the Debye function is used to estimate Clat in the full temperature range. The following expression was used to fit the experimental curve apart from C_m

$$C_{el}(T)+C_{lat}(T)=\gamma T+9nR\left(\frac{T}{\theta_D}\right)^3\int_0^{x_D}\frac{x^4e^x}{(e^x-1)^2}dx \qquad (1)$$

With γ the Sommerfield coefficient, θ_D the Debye temperature and $x_D=\theta_D/T$. By adjusting the curve, a good fit represented by full line in Fig. 6 can be obtained. It was reached with the following parameters: γ=100 mJ mol^{-1} K^{-2} and θ_D=210 K; this last temperature is coherent with those reported for other Gd based materials like GdMg (θ_D=228 K) [32] and $Gd_5Si_2Ge_2$ (θ_D=250 K) [33]. The magnetic contribution C_m, plotted in the inset of Fig. 6, was deducted as follows: $C_m=C_p-(C_{el}+C_{lat})$. The two peaks at 165 and 295 K appear clearly on the C_m *versus* T curve. The C_m value attributed to the magnetic transition of Gd_5CoSi_2 was estimated at $C_m^{peak}\sim$97 J mol^{-1} K^{-1} at the edge of the λ peak at 165 K. Therefore, with five Gd^{3+} ions per unit formula of Gd_5CoSi_2, the value corresponding to each one is $C_m(Gd^{3+})\sim$19.4 J (Gd^{3+})mol^{-1} K^{-1}. This value is in good agreement with that of 20.15 J (Gd^{3+})mol^{-1} K^{-1} predicted by Blanco et al. [34] for simple ferromagnetic structure using a mean-field model.

The evolution of the magnetic entropy S_m *versus* T can then be calculated with the equation:

$$S_m(T)=\int_0^T\frac{C_m(T)}{T}dT \qquad (2)$$

The temperature dependence of S_m, presented in Fig. 7, shows a pronounced increase of S_m after the ferromagnetic ordering temperature (T_C=165 K) of Gd_5CoSi_2. The S_m value is 12.2 J (Gd)mol^{-1} K^{-1} at T_C and 13.9 J (Gd)mol^{-1} K^{-1} at 312 K, respectively, 71% and 80% of the theoretical value R ln(2J+1)=17.3 J (Gd)mol^{-1} K^{-1} for one mole of Gd^{3+} (J=7/2). It indicates some persistent magnetic interaction after T_C, which is in correlation with the presence of the parasite ferromagnetic phase $Gd_6Co_{1.67}Si_3$.

Isothermal field dependence of magnetization M measurements were performed with decreasing magnetic field from 4.6 to 0 T and for various temperatures between 10 and 310 K (Fig. 8); no remanence was evidenced. At 10 K, M saturates at 4.6 T and reaches 6.8 μ_B as magnetic moment per Gd^{3+}, which is slightly smaller than the theoretical value for a free Gd^{3+} ion, g_JJ=7 μ_B (g_J being the Landé factor and J the total angular momentum). Finally, we must notice that the variation of M *versus* the applied field tends to linearity only above 310 K (temperature higher than Curie temperature of the impurity $Gd_6Co_{1.67}Si_3$), as expected.

The isothermal magnetic entropy change ΔS_m was determined from the magnetization data (Fig. 8) by integrating Maxwell relation:

$$\Delta S_m(T,\Delta H)=\int_{H_0}^{H_f}\left(\frac{\partial M(T,H)}{\partial T}\right)_H dH \qquad (3)$$

The results for Gd_5CoSi_2, in applied fields of ΔH=2 and 4.6 T, are reported in Fig. 9(a). A rather high peak centered between 165 and 175 K is observed, i.e. around the Curie temperature of this compound, as expected for the magnetocaloric effect. ΔS_m reaches the maximum value of −8.7 J K^{-1} kg^{-1} at 4.6 T and −4.7 J K^{-1} kg^{-1} at 2 T.

The adiabatic temperature change ΔT_{ad} was determined by combining the heat capacity measurements at zero field (Fig. 6) and the magnetization data (Fig. 8) *via* the following equation proposed by Foldeaki et al. [35], which neglects the dependence of C_p over the applied field H:

$$\Delta T_{ad}(T)=-\frac{T}{C_p(T)_{H=0}}\Delta S_m(T)_{\Delta H} \qquad (4)$$

ΔT_{ad} *versus* T for Gd_5CoSi_2 is plotted in Fig. 9(b) for ΔH=2 and 4.6 T. As expected, a peak near the Curie temperature of the ternary silicide is observed, with a maximum of ΔT_{ad} about 3.1 and 5.9 K for ΔH=2 and 4.6 T, respectively. The procedure for the indirect calculation of ΔT_{ad}, described as the most accurate by Pecharsky et al. [36], consisting in the use of the heat capacity measurement to calculate the total entropy at constant field gave the same ΔT_{ad} *versus* T curve than this one. Indeed, due to the fact that C_p was measured at zero magnetic field only, it is impossible to get a more accurate estimation of ΔT_{ad} whatever the calculation method applied.

The ΔS_m^{peak} values reported here for Gd_5CoSi_2 are compared to that of other magnetocaloric materials existing in the ternary Gd–Co–Si system (Table 3). It appears that this new ternary silicide compares well with $Gd_{12}Co_7$ of which T_C=163 K is really close to that of Gd_5CoSi_2, and which was the most efficient material with a paramagnetic to ferromagnetic transition in this system so far. Absolute values for pure Gd are still a little higher, but when expressed per weight amount of Gd, they get really close. Finally, only Gd_3Co, with its metamagnetic transition at 128 K still has the most elevated ΔS_m^{peak} values, but at a lower temperature.

4. Conclusion

The investigation of the system Gd–Co–Si in the rich part in gadolinium has highlighted a new ternary silicide Gd_5CoSi_2. This compound obtained after annealing at 1003 K, adopts a disordered tetragonal structure deriving from the Cr_5B_3-type. This structure is different to that reported for the binary compound Gd_5Si_3 (hexagonal, Mn_5Si_3-type), which is in equilibrium with Gd_5CoSi_2 at 1003 K. The ternary silicide presents ferromagnetic ordering at 168 K that could be associated to a very interesting magnetocaloric effect of 5.9 K in a magnetic field change of 4.6 T. This result encourages us to consider in the future other compounds RE_5CoSi_2, with for instance RE=Nd, Tb.

Acknowledgments

The authors are indebted to the Conseil Régional d'Aquitaine for financial support, especially C. M. for a Ph.D. grant.

References

1 S. Yu, A.M. Dan'kov, V.K. Tishin, Pecharsky and K.A. Gschneidner Jr., Phys. Rev. B 57 (1998), pp. 3478–3490.
2 V.K. Pecharsky and K.A. Gschneidner Jr., Phys. Rev. Lett. 78 (1997), pp. 4494–4497.
3 V.A. Cherchenko, E. Cesari, V.V. Kokorin and I.N. Vitenko, Scr. Metall. Mater. 33 (8) (1995), pp. 1239–1244.
4 G.H. Wen, R.K. Zheng, X.X. Zhang, W.H. Wang, J.L. Chen and G.H. Wu, J. Appl. Phys. 91 (10) (2002), pp. 8537–8539.
5 E. Gaudin, F. Weill and B. Chevalier, Z. Naturforsch. 61b (2006), pp. 825–832.
6 E. Gaudin, S. Tencé, F. Weill, J. Rodriguez-Fernandez and B. Chevalier, Chem. Mater. 20 (2008), pp. 2972–2979.
7 B. Chevalier, E. Gaudin and F. Weill, J. Alloys Compd. 442 (2007), pp. 149–151.
8 S. Tencé, E. Gaudin, G. André and B. Chevalier, J. Phys. D: Appl. Phys. 42 (2009), p. 165003.
9 E. Gaudin, S. Tencé and B. Chevalier, Solid State Sci. 10 (2008), pp. 481–485.
10 S. Tencé, E. Gaudin and B. Chevalier, Intermetallics 18 (2010), pp. 1216–1221.
11 S.N. Jammalamadaka, N. Mohapatra, S.D. Das, K.K. Iyer and E.V. Sampathkumaran, J. Phys.: Condens. Matter 20 (2008), p. 425204.
12 J. Shen, J.F. Wu and J.R. Sun, J. Appl. Phys. 106 (2009), p. 083902.
13 J. Shen, Y.X. Li, Q.Y. Dong, F. Wang and J.R. Sun, Chin. Phys. B 17 (2008), pp. 2268–2271.
14 N. Mohapatra, S.N. Jammalamadaka, S.D. Das and E.V. Sampathkumaran, Phys. Rev. B 78 (2008), p. 054442.
15 A. Haldar, N.K. Singh, K.G. Suresh and A.K. Nigam, Physica B 405 (2010), pp. 3446–3451.
16 J. Shen, F. Wang, Y.X. Li, J.R. Sun and B.G. Shen, Chin. Phys. 16 (2007), pp. 3853–3857.
17 J. Shen, Y.X. Li and J.R. Sun, J. Alloys Compd. 476 (2009), pp. 693–696.
18 S. Wu, J. Yan, L. Zhang, W. Qin, L. Zeng and Y. Zhuang, Z. Metallkd 91 (2000), pp. 373–374.
19 V. Petricek, M. Dusek and L. Palatinus Jana, Jana 2006. The Crystallographic Computing System Jana, Institute of Physics, Praha, Czech Republic (2006).
20 V. Babizhetskyy, J. Roger, S. Députier, R. Jardin, J. Bauer and R. Guérin, J. Solid State Chem. 177 (2004), pp. 415–424.
21 O.A.W. Strydom and L. Alberts, J. Less-Common Met. 22 (1970), pp. 511–515.
22 J. Roger, V. Babizhetskyy, R. Jardin, J.-F. Halet and R. Guérin, J. Alloys Compd. 415 (2006), pp. 73–84.
23 D. Gout, E. Benbow and Gordon J. Miller, J. Alloys Compd. 338 (2002), pp. 153–164.
24 A.V. Tkachuk, H. Bie and A. Mar, Intermetallics 16 (2008), pp. 1185–1189.
25 Y. Mozharivskyj and H.F. Franzen, J. Solid State Chem. 152 (2000), pp. 478–485.
26 Yu Verbovytsky and K. Latka, J. Alloys Compd. 438 (2007), pp. L4–L6.
27 D. Hohnke and E. Parthe, J. Less-Common Met. 17 (1969), pp. 291–296.
28 W.B. Pearson, The Crystal Chemistry and Physics of Metals and Alloys, Wiley, New York (1972).
29 F. Canepa, S. Cirafici and M. Napoletano, J. Alloys Compd. 335 (2002), pp. L1–L4.
30 J. Szade and M. Drzyzga, J. Alloys Compd. 299 (2000), pp. 72–78.
31 V. Svitlyk, F. Fei and Y. Mozharivskyj, J. Solid State Chem. 181 (2008), pp. 1080–1086.
32 U. Kobler, R.M. Mueller, W. Schnelle and K. Fischer, J. Magn. Magn. Mater. 188 (1998), pp. 333–345.
33 O. Svitelskiy, A. Suslov, D.L. Schlagel, T.A. Lograsso, K.A. Gschneidner Jr. and V.K. Pecharsky, Phys. Rev. B 74 (2006), p. 184105.
34 J.A. Blanco, D. Gignoux and D. Schmitt, Phys. Rev. B 43 (1990), pp. 13145–13151.
35 M. Foldeaki, R. Chahine, B.R. Gopal, T.K. Bose, X.Y. Liu and J.A. Barclay, J. Appl. Phys. 83 (1998), p. 2727.

36 V. Pecharsky and K.A. Gschneidner Jr., J. Appl. Phys. 86 (1999), pp. 565–575.
37 X. Chen and Y.H. Zhuang, Solid State Commun. 148 (2008), pp. 322–325.
38 S.K. Tripathy, K.G. Suresh and A.K. Nigam, J. Magn. Magn. Mater. 306 (2006), pp. 24–29.
39 Q. Zhang, B. Li, X.G. Zhao and Z.D. Zhang, J. Appl. Phys. 105 (2009), p. 053902.

Figures :

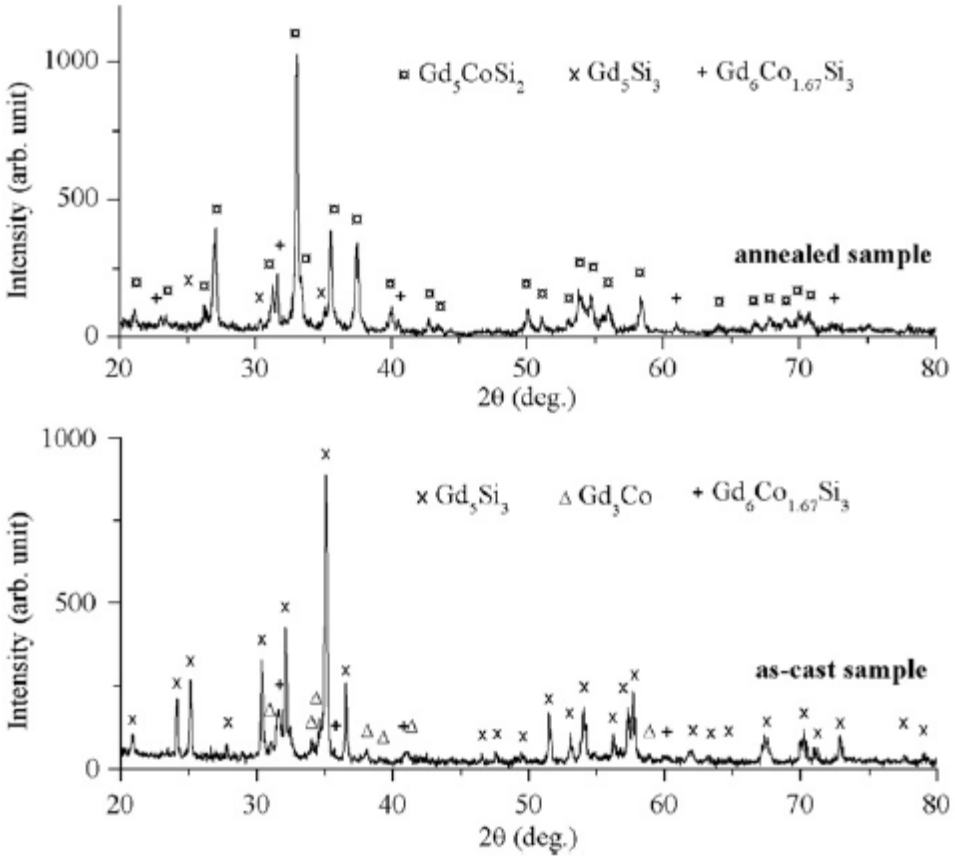

Fig. 1. X-ray powder patterns of Gd_5CoSi_2 sample after melting (as-cast) followed by annealing at 1003 K (annealed). The phases are identified by symbols as indicated on top of the patterns.

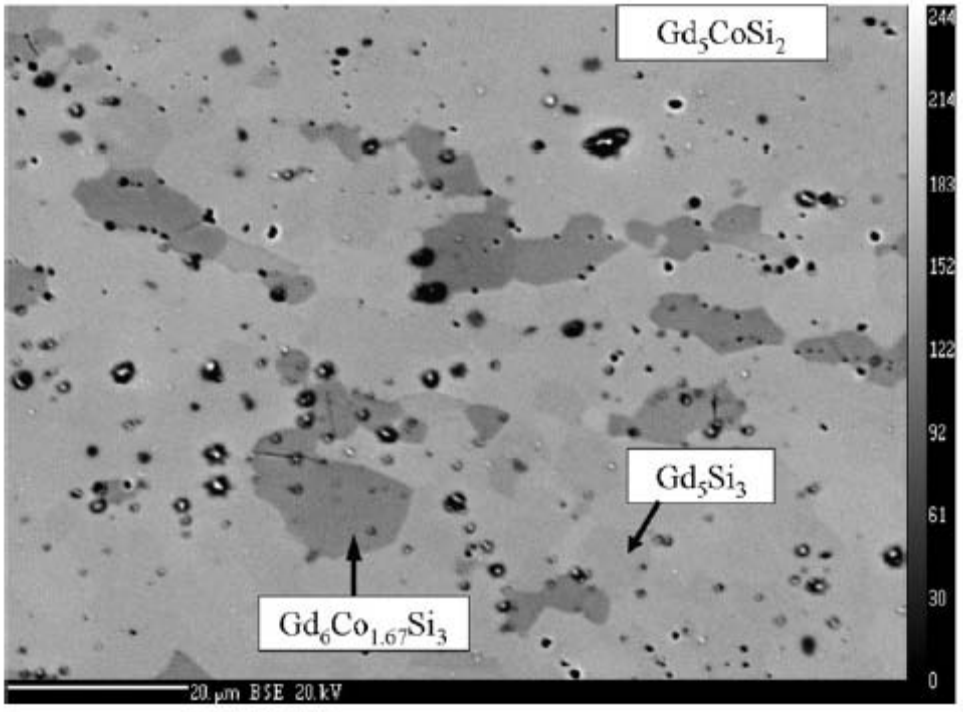

Fig. 2. Microstructure of the annealed sample. The main phase Gd_5CoSi_2 and the impurities Gd_5Si_3 and $Gd_6Co_{1.67}Si_3$ are indicated. The black round areas correspond to the opened porosities.

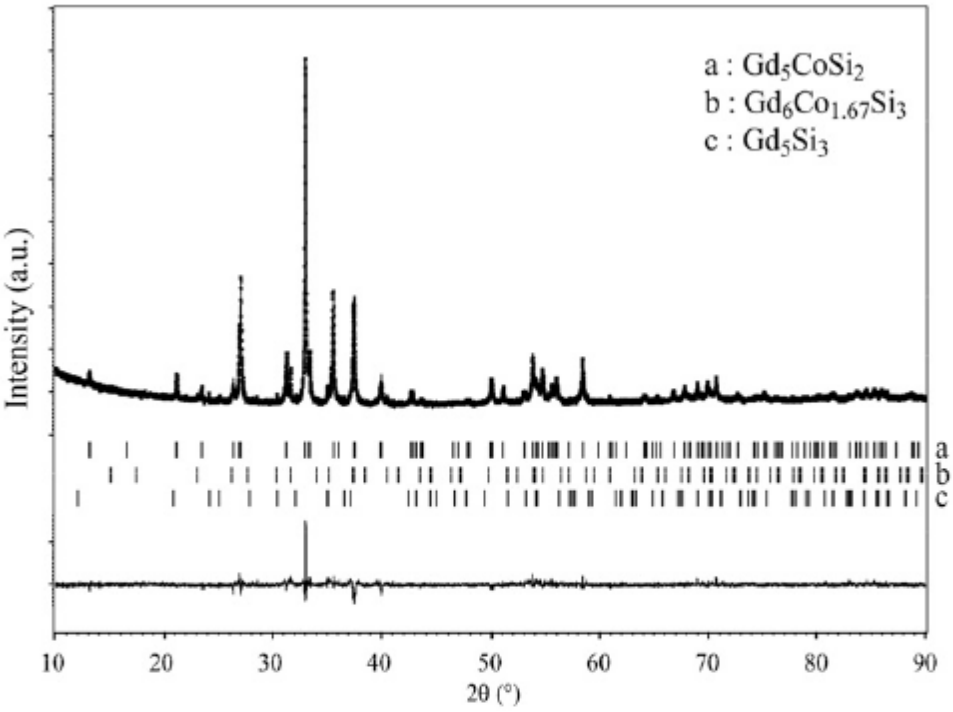

Fig. 3. Rietveld refinement of Gd_5CoSi_2 (annealed sample) XRD powder pattern measured with Cu-Kα_1 radiation ($\lambda = 1.54051$ Å) at $T = 293$ K (observed (cross), calculated (full line), and difference (bottom) profiles). For the sake of clarity, only the angle range 10–90 was displayed, no Bragg peaks are observed below 10°. The Bragg peak positions are indicated by tick marks for the Gd_5CoSi_2 (a) main phase and the impurities $Gd_6Co_{1.67}Si_3$ (b) and Gd_5Si_3 (c).

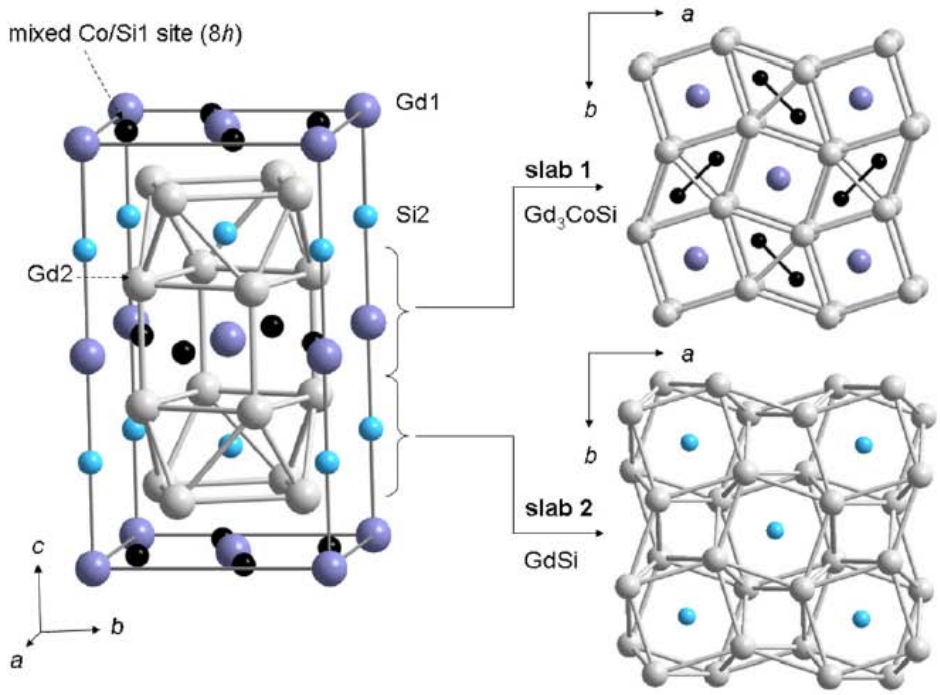

Fig. 4. Structure of Gd_5CoSi_2 with the tetragonal Cr_5B_3-type, built as a stacking of two types of slabs along the *c*-axis (the slab 1 corresponds to Gd_3CoSi and the slab 2 to GdSi). Co atoms fill half of the 8*h* sites located in slab 1 (black circles).

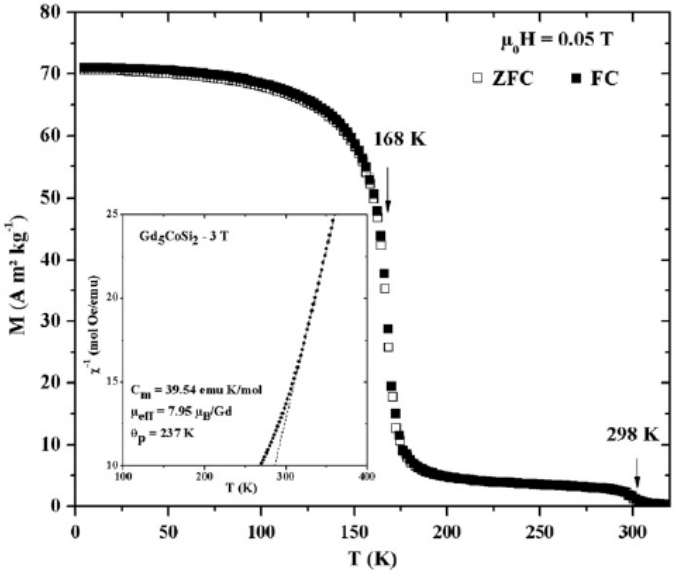

Fig. 5. Temperature dependence of the magnetization M of Gd_5CoSi_2 (annealed sample) measured with an applied field of 0.05 T (open and closed symbols correspond, respectively, to the zero-field cooled (ZFC) and field cooling (FC) processes). The inset displays its reciprocal magnetic susceptibility χ_m^{-1} *versus* temperature (the dashed line follows Curie Weiss law).

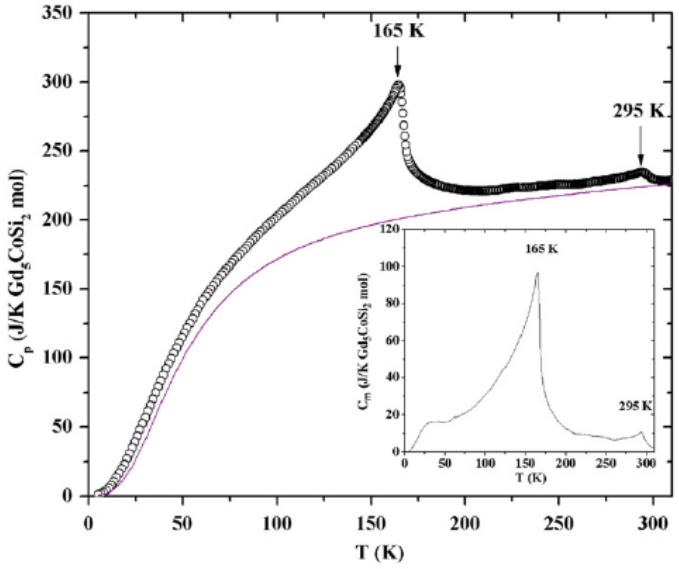

Fig. 6. Temperature dependence of the heat capacity C_p of Gd_5CoSi_2 (annealed sample) between 5 and 310 K. The line represents the sum of the electronic (γ=100 mJ mol^{-1} K^{-2}) and lattice (θ_D=210 K) contributions. Inset shows the temperature dependence of the magnetic contribution C_m.

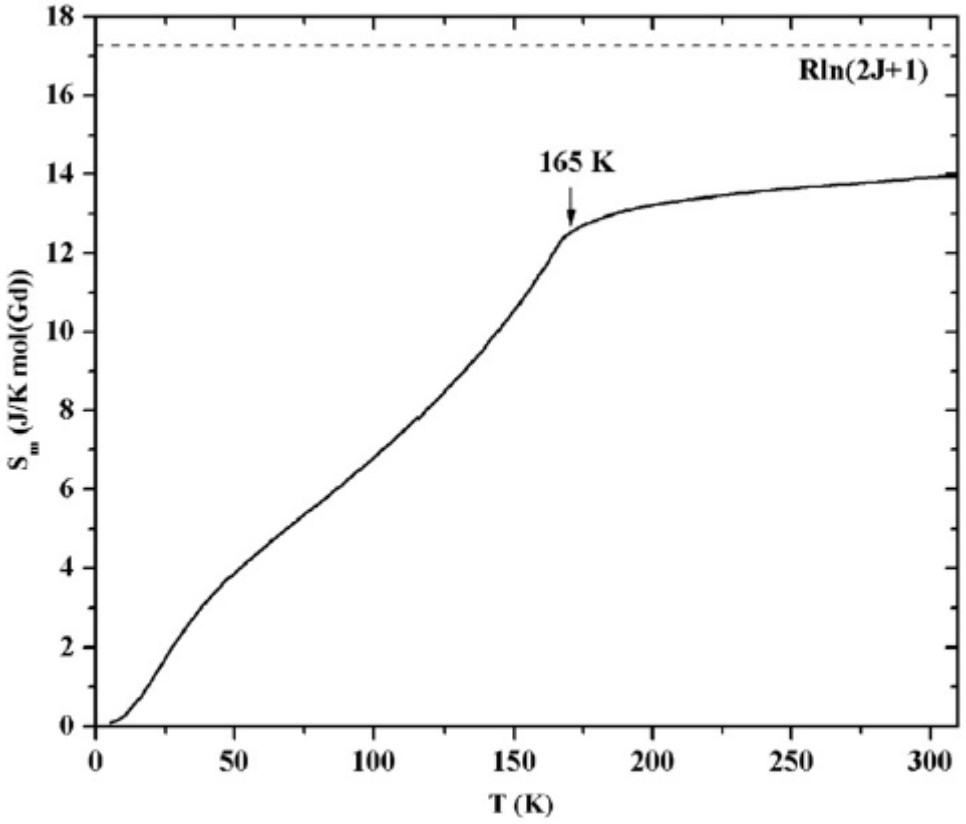

Fig. 7. Temperature dependence of the magnetic entropy S_m of Gd_5CoSi_2 (annealed sample). The dashed line represents the theoretical limit R ln(2J+1) with J=7/2 for Gd^{3+} ions.

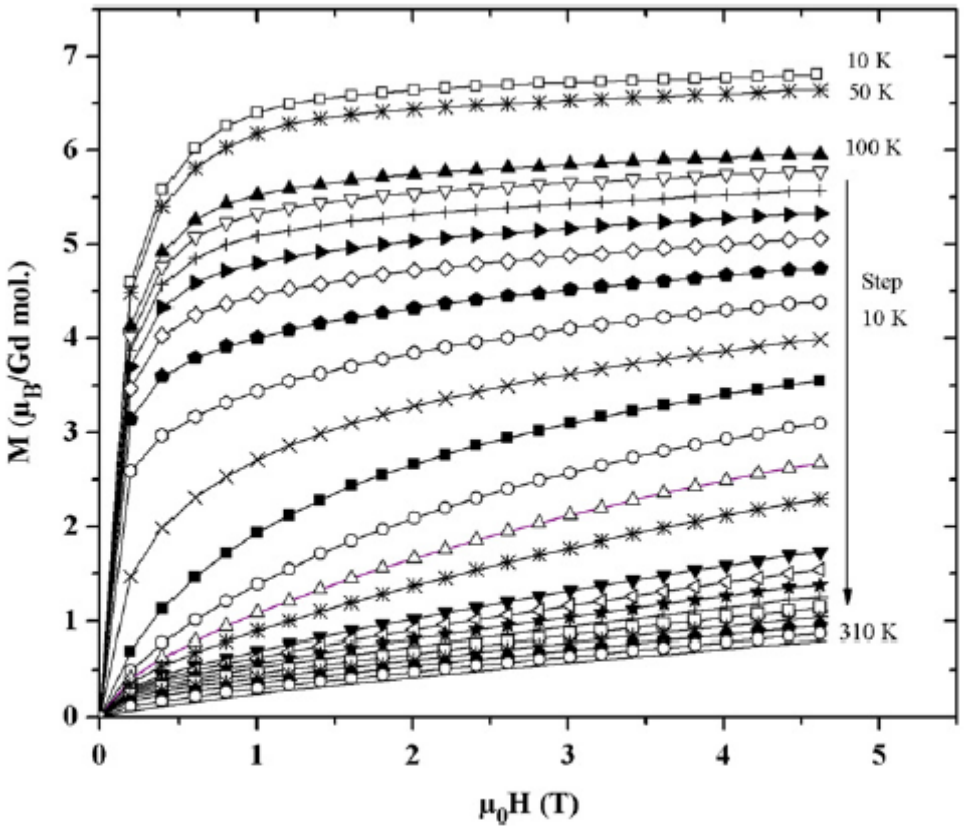

Fig. 8. Field dependence of the magnetization M of Gd_5CoSi_2 (annealed sample) measured at various temperatures.

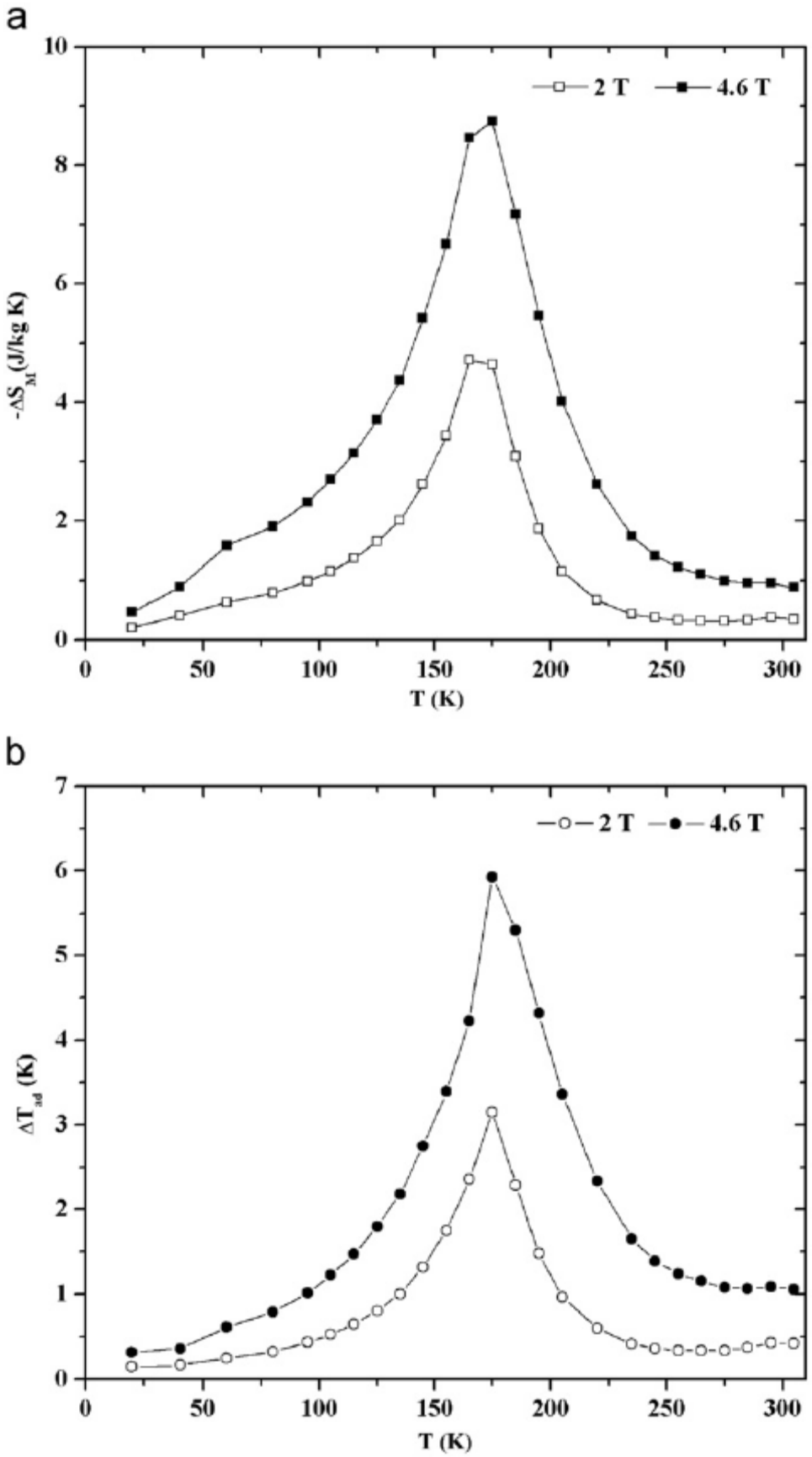

Fig. 9. Temperature dependence of (a) the isothermal magnetic entropy change ΔS_m and (b) the adiabatic temperature change ΔT_{ad} for Gd_5CoSi_2 (annealed sample) at 2 and 4.6 T.

Tableaux :

Table 1
Atomic coordinates and isotropic displacement parameters (Å^2) for Gd_5CoSi_2[a].

Atom	Site	Occup.	x	y	z	U_{iso} (Å^2)
Gd1	4*c*	1	0	0	0	0.014(6)
Gd2	16*l*	1	0.1683(5)	x+1/2	0.1438(4)	0.006(4)
Si1	8*h*	1/2	0.383(2)	x+1/2	0	0.010(8)[b]
Co	8*h*	1/2	0.383(2)	x+1/2	0	0.010(8)[b]
Si2	4*a*	1	0	0	1/4	0.010(8)[b]

[a] Space group *I*4/*mcm*, a=7.5799(4) and c=13.5091(12) Å.
[b] Constrained to be equal.

Table 2
Number of neighbours and interatomic distances (Å) in Gd_5CoSi_2.

Gd1:	4Si1/Co	3.036(15)
	2Si2	3.3773(6)
	8Gd2	3.424(5)
Gd2:	2Si1/Co	2.933(13)
	1Si1/Co	3.012(13)
	2Si2	3.163(5)
	1Gd2	3.362(9)
	2Gd1	3.424(5)
	1Gd2	3.608(5)
	2Gd2	3.840(8)
	1Gd2	3.885(10)
	4Gd2	3.987(5)
Si1/Co:	1Si1/Co	2.51(2)
	4Gd2	2.933(13)
	2Gd2	3.012(13)
	2Gd1	3.036(15)
Si2:	8Gd2	3.163(5)
	2Gd1	3.3773(6)

Table 3
Curie (T_C) or Néel (T_N) temperatures and maximum isothermal magnetic entropy change ΔS_m^{max} reported in the literature for compounds in the system Gd–Co and for $Gd_6Co_{1.67}Si_3$. $\Delta S_{m/Gd}^{max}$ is the maximum isothermal magnetic entropy per weight amount of gadolinium in the sample.

		ΔS_m^{max} (J kg^{-1} K^{-1})	$\Delta S_{m/Gd}^{max}$ (J kg$_{(Gd)}^{-1}$ K^{-1})	ΔH (T)	Reference
Gd_5CoSi_2	T_C=168 K	−4.7	−5.4	2	This work
		−8.7	−10.0	4.6	
$Gd_6Co_{1.67}Si_3$	T_C=294 K	−2.9	−3.5	2	[6]
		−5.7	−6.8	4.8	
Gd	T_C=294 K	−5.5	−5.5	2	[1]
		−10.3	−10.3	5	
$Gd_{12}Co_7$	T_C=163 K	−4.6	−5.6	2	[37]
Gd_3Co	T_N=128 K	−11.0	−12.4	5	[38]
Gd_4Co_3	T_C=220 K	−2.7	−3.5	2	[39]
		−5.7	−7.3	5	
$Gd_6Co_{4.85}$	T_C=219 K	−2.4	−3.1	2	[10]
		−4.8	−6.3	4.5	